

**UNIVERSITY OF NAPLES FEDERICO II**



**PH.D. PROGRAM IN**  
**CLINICAL AND EXPERIMENTAL MEDICINE**  
*CURRICULUM IN ODONTOSTOMATOLOGICAL SCIENCES*

**XXXIV Cycle**  
*(Years 2018-2021)*

**Chairman: Prof. Francesco Beguinot**

**PH.D. THESIS**

**TITLE**

**DESIGN STRATEGIES TOWARDS THE DEVELOPMENT OF  
ADVANCED SYSTEMS AND DEVICES IN CLINICAL AND  
EXPERIMENTAL MEDICINE**

TUTOR

**Prof. Vincenzo D'Antò**  
**Prof. Roberto De Santis**

PH.D. STUDENT

**Dr. Vito Gallicchio**

# 1. Introduction

In the current PhD thesis different topics related to the dentistry field have been studied and analyzed. First, the focus has been devoted to the design of advanced devices for bone tissue regeneration during the orthodontic movement. In this area there is a particular attention to reduce the orthodontic treatment time by speeding up the tooth movement since, generally, the aforementioned treatment takes an average time of 18-24 months. A promising approach may be given by the coupling of static magnetic fields (SMFs) and non-ionizing electromagnetic fields (EMFs) with advanced devices in the form of “solid” 3D additive manufactured magnetic scaffolds and/or injectable gels to improve cell activity by enhancing cell signaling and guiding cell migration, proliferation and differentiation. This approach would be possible thanks to the use of magnetic nanoparticles (e.g., Fe<sub>3</sub>O<sub>4</sub>) that show a superparamagnetic behavior.

Different studies have also been carried out in the conservative dentistry field by engineering technical solutions as well as by testing and analyzing polymers, composites and biological tissues, in terms of mechanical properties, thermal properties and surface/interface adhesion. These studies would be useful to define new clinical procedures and to analyze the long-term effects of dental materials, endodontic fiber-reinforced posts and reconstruction techniques on the success of dental restorations.

## **Chapter 3**

# **Fracture strength and failure modes of endodontically treated premolars restored with compact and hollow composite posts subjected to cyclic fatigue**

## **1. Introduction**

The main goal of conservative dentistry is to preserve teeth and to reduce extractions as much as possible. Endodontic treatment is the gold standard to prevent decayed teeth from extraction although endodontically treated teeth are prone to fracture [1, 2]. The fracture can be caused by the pulpar roof loss produced by endodontic access, and even carious process can remove the remaining tooth structure, weakening it. First maxillary premolars have a high incidence of fractures due to the small root diameter. Premolars are subjected to higher lateral forces during mastication compared to the anterior teeth. Such elements often require cusp coverage and indirect reconstruction techniques (overlays, crowns), while direct restoration is intended for cases in which vestibular and palatal cusps are well represented and at least one marginal ridge is present [3].

Physical and mechanical properties of post-endodontic restorations are relevant to increase the retention and resistance of the tooth restoration system. Several studies have demonstrated that the use of endodontic post increases the material build up core retention, depending on the rigidity of the material of post core systems [4, 5, 6]. A property of great importance for composite materials is strength that gives information

on the amount of force the material can withstand and so the ability to react to external loads. Generally, when two or more materials with different rigidities are coupled the stress is not uniformly distributed, and the major stress is being transferred from the rigid material to the compliant one [7]. Strength and rigidity are the key to balance the stress distribution between materials, and in the last years research has focused on the development of fiber posts with a trade-off between rigidity and compliance [8]. In particular, fiber posts goal is to achieve an elastic modulus similar to that of dentin, allowing to have a mechanically homogeneous system [9]. From the latest 90's carbon fiber and glass fiber posts are available on the market to replace highly rigid metal posts. These posts present an elastic modulus similar to that of dentin and the stress transferred to the nearest tissues is distributed uniformly, thus preventing root fractures frequently observed in metal post restored teeth [10]. The bond strength between the resin luting agent and the root canal surface is influenced by the polymerization degree of resin cement in the post cavity. Specifically, a lower polymerization degree can be found at the bottom of the cavity due to the decrease of light cure intensity [11]. Lately, self-adhesive resin cement characterized by a dual-cure mechanism and no dentin pre-treatment requirement has been introduced on the dental market [12]. The presence of two residual marginal ridges significantly improves long term success of post-endodontic restorations [13]. A prospective in vivo study showed similar 3-year survival rates between endodontically treated premolars restored with fiber posts and direct composite resin and complete restorations with metal ceramic crowns [14]. Nowadays a new type of post is available on the dental market, the hollow fiber post

[15]. Fiber reinforced hollow posts represent an advancement of compact fiber posts. In particular, the main advantage of hollow posts is the reverse extrusion of the luting cement involving an application of the cement from the apex to the crown of the tooth to be restored. Thanks to this technique, the cementation process is optimized by avoiding the entrapment of air bubbles and the stability of the hollow post is improved by the presence of the cement in the cavity of the post itself. Currently, there is insufficient evidence of fracture resistance and fracture patterns in endodontically treated teeth to define the proper use of fiber posts, especially when teeth are subjected to thermomechanical aging and simulation of masticatory forces as in the oral environment [16]. It has been shown that in vitro the reduced stiffness of certain fiber-reinforced posts may be beneficial in preventing catastrophic root fractures [17]. However, it is not clear whether fiber-reinforced posts can actually provide adequate support for a core. The deformation of a fiber-reinforced post may result in greater stress on the composite core, causing premature failure of the core restoration [18]. This problem is of particular clinical interest in the cases where little or no coronal tooth structure remains. The aim of the current study was to evaluate the fracture resistance and fracture patterns of endodontically treated maxillary premolars subjected to mesial-occlusal-distal (MOD) cavities restored using a resin composite core with different types of fiber posts under cyclic loading.

## **2. Materials and Methods**

Three endodontic posts, a hollow carbon fiber post (HCP), a hollow glass fiber post (HGP), a compact glass fiber post (GP), and the self-etching and self-adhesive dual

cement Maxcem Elite Chroma (MEC) were used. Details of the selected posts and cements are reported in Table 1.

**Table 1.** Composition and geometrical details of endodontic composite posts and cement. R and r represent the external and internal radius of hollow posts, respectively.

<b>Materials</b>	<b>Manufacturer</b>	<b>Code</b>	<b>Composition</b>	<b>R [mm]</b>	<b>r [mm]</b>
<b>Hollow Carbon Post</b>	Isasan (Italy)	HCP	- Carbon fibers 60% - Bisphenol-A + methyloxirane 40% - Barium sulfate traces	1.2	0.5
<b>Hollow Glass Post</b>	Isasan (Italy)	HGP	- Silica fibers 55% - Diphenylpropane + methyloxirane 45%	1.2	0.5
<b>Glass Post</b>	Isasan (Italy)	GP	- Silica fibers 55% - Diphenylpropane + methyloxirane 45%	1.2	
<b>Maxcem Elite Chroma</b>	Kerr (USA)	MEC	- 2-hydroxyethyl methacrylate - 2-hydroxy-1,3-propanediyl bismethacrylate - 7,7,9 (or 7,9,9) trimethyl-4, 13-dioxo-3, 14-dioxa-5, 12-diazahexadecane-1, 16-diyl bismethacrylate	Square cross-section 1x1 mm <sup>2</sup>	

			-Propylidynetrimethanol, ethoxylated, esters with acrylic acid - Ytterbium trifluoride	
--	--	--	---	--

Three-point bending tests were performed on each sample of endodontic posts using the Instron 5566 dynamometer equipped with a load cell of 100 N. The span (L) was set at 13 mm and bending tests were carried out at a speed of 1 mm/min. Each sample consisted of 10 specimens.

The Maxcem Elite Chroma cement was tested in the same fashion of endodontic posts. Dental cement specimen bars were photo-cured in Teflon moulds as previously described [11]. Briefly, the cement was injected into a prismatic cavity mould having a cross section of 1x1 mm<sup>2</sup>, and a Mylar strip was used to cover the mould and to avoid the composite oxidation during the curing process. The Swiss Master Light (EMS) curing unit at an intensity of 1000 mW/cm<sup>2</sup> was employed. The curing unit and the mould containing the cement were fixed onto a modified 3D CAD/CAM system [19] in order to provide a continuous curing process along the whole length of the specimen bar (15 mm), and the process was performed within 20 s of light exposure.

A sample consisting of ten specimens of hollow carbon fiber post filled with Maxcem Elite Chroma cement (HCP+MEC) was also considered. The cement was injected into the cavity of the hollow carbon fiber post. A curing process for 20 s was considered and specimens were stored in a dry and dark environment for 72 h in order to allow the polymerization of the dual cement. A sample consisting of ten specimens

of hollow glass fiber post filled with Maxcem Elite Chroma cement (HGP+MEC) was also prepared in a similar fashion.

The bending behavior of HCP, HCP+MEC, GP, HGP, HGP+MEC and MEC was described through load-displacements curves. The steepness of the linear portion of each curve was computed through the best linear curve fit using the Kaleidagraph software [Synergy Software, Reading, Pennsylvania, USA]

The Young's modulus (E) of each material was computed using the following equation:

$$\frac{dP}{dy} = \frac{48 EI}{L^3} ; \quad (1)$$

where P is the applied load, y the displacement of the middle-span cross-section, L is the span and I is the second moment of area. The product EI is known as bending stiffness.

The second moment of area of compact posts (i.e. GP), hollow posts (i.e. HCP and HGP) and cement (MEC) were computed according to the following equations:

$$I = \frac{\pi}{4} R^4 \quad ; \quad I = \frac{\pi}{4} (R^4 - r^4) \quad ; \quad I = \frac{b^4}{12} \quad ; \quad (2)$$

where R, r and b were the external post's radius, the internal post's radius and the thickness of cement bar, respectively.

For hollow posts filled with cement (i.e. HCP+MEC and HGP+MEC) the below reported equation was used to verify the experimental linear behavior with the theoretical response, once the Young's moduli of the single components were experimentally computed:

$$\frac{dP}{dy} = \frac{48}{L^3} (E_e I_e + E_i I_i) \quad ; \quad (3)$$

where  $E_e$  and  $I_e$  are the Young's modulus and the second moment of area of the external composite shell, respectively. While  $E_i$  and  $I_i$  represent the Young's modulus and the second moment of internal cement core, respectively.

On the other hand, the axial stiffness of each sample is obtained by the product of the area of the specimen cross-section and the Young's modulus. For HCP+MEC and HGP+MEC the axial stiffness is given by  $E_e \cdot A_e + E_i \cdot A_i$ , where  $A_e$  and  $A_i$  are the cross-section of the external shell and the internal core, respectively.

Fifty maxillary first premolars were selected. Teeth were extracted for orthodontic reasons. The study was approved by the Ethics Committee of the University of Naples Federico II, with protocol number 137 2017. Inclusion criteria were no carious tissue, similar crowns and roots sizes, two root canals, no abfractions, no cracks, no erosions. Teeth were placed in 5% NaOCl solution for 5 minutes and stored in physiological solution at room temperature to prevent dehydration.

Three endodontic posts, a hollow carbon fiber post, a hollow glass fiber post and a compact glass fiber post, were used. Teeth restored with posts were compared with control teeth restored using resin-based composite and with healthy sound teeth. Teeth were subjected to fatigue testing or loading and finally compression tests to evaluate the fracture resistance and fracture patterns.

Specimens were subjected to endodontic treatment except the control group (healthy teeth). Cavity access was prepared with a diamond spheric bur mounted on the turbine Fona8080 (Fonadental, Assago, Italy). Canals were scouted at work length

using k-file 10 (kerr corporation). Glide path was performed using pro-glider (Maillefer, Swiss). Canals were instrumented by using crown down technique with rotating files ProTaper next x1-x2 taper 0.04 (Maillefer, Swiss). After each file change, canals were irrigated with 2.5% NaOCl solution. Root canals were dried with size 25 paper points and obturated with gutta-percha cones using single-cone technique. The samples were stored at 37 °C and 100% humidity. All teeth were manually prepared by an experienced operator. Samples were randomly divided into five groups (n = 10) as shown below and different fiber posts were employed for the restoration.

### **Group 1**

Teeth in this group served as control group (n=10) and they were not subjected to any procedure.

### **Group 2**

Class 2 mesio-occlusal-distal cavities were prepared with gingival margin at the cement-enamel junction level. The thickness of the bucco-lingual cavity was 3 mm measured with a digital caliper (Mitutoyo, Takatsuku, Japan). Teeth were then subjected to an adhesive procedure by acid etching of enamel and dentin for 30 s and 15 s, respectively, using 37% phosphoric acid (Gerhò, Bolzano, Italy) and subsequently 5 s of rinsing and drying; finally, the application of the Optibond SE (Kerr Corporation) adhesive system and photo-curing with the Swiss Master Light (EMS) curing unit at an intensity of 1000 mW/cm<sup>2</sup> [20]. SonicFill was directly dispensed into dental cavities using the Sonicfill handpiece.

### **Group 3**

Palatal Root canals were subjected to post space preparation. Tech21 compact glass fiber post (Isasaan, Como, Italy) was inserted in post-endodontic restoration. Post housing was prepared in the palatal canal using the Gates Glidden bur n. 4 and then fiber posts were inserted. The self-etching and self-adhesive dual cement Maxcem Elite Chroma (Kerr corporation) were used for luting fiber posts, according to manufacturer's instructions. Tech21 posts were immersed in the cement and inserted into the canal. Maxcem was placed into the post spaces using a Lentulo spiral or drill (Dentsply Sirona Germany). Light curing was performed using the Swiss Master Light (EMS, Switzerland) curing unit at 800 mW/cm<sup>2</sup> for 40 seconds. After post cementation, teeth were restored with direct restoration using composite. Restorations were done as in Group 2.

#### **Group 4**

Post space and restorations were done as in Group 3, except for the cementation and type of post. Techole (Isasaan, Como, Italy) hollow glass fiber post was inserted in post-space restoration. While Tech21 posts were immersed in the cement and inserted into the canal, Techole posts were inserted into the canal and cement was then applied through the central hole, thus flowing through the entire Techole post up to its extremity. Therefore, by using these posts it is no longer necessary to first fill the canal with the cement and then insert the post. Instead, everything is accomplished in one single step, during which the post is simultaneously an instrument which is able to guide the cement into the canal. After post cementation, teeth were restored with direct restoration using composite as done in previous groups.

## **Group 5**

With regard to this group, the same procedures as in Group 4 were applied. The only difference consisted in the use of Techole hollow carbon fiber post.

Premolars were cemented in aluminum cylinders (D=16 mm) using a low temperature self-curing acrylic resin 2 mm below their cementum-enamel junction (CEJ) to simulate crestal bone.

Then, specimens were subjected to fatigue stress cyclic loading for one million cycles with a sinusoidal variable loading in the range 10-100 N at a frequency of 2 Hz. After fatigue cycles, teeth were subjected to compression tests using the Instron 5566 testing machine at a speed of 1 mm/min. The dynamometer compliance was experimentally measured and the compression stiffness was evaluated through the steepness of the stress–strain curve in the elastic region. Finally, data were statistically analyzed using two-way ANOVA followed by Tukey’s test at a critical value of 0.05. The mean and standard deviation (SD) of fracture resistance in each group were calculated.

Optical and scanning electron microscopy (SEM) were used to study fracture behavior of teeth that underwent cyclic fatigue and static tests to failure. The optical microscope Motic AE21 (Motic Ltd., Kowloon, Hong Kong) equipped with a Nikon D3200 camera was implemented to investigate at a macroscale level the type of fracture pattern. Fracture propagating from the crown to e level below the CEJ was considered unfavorable, as they cannot be restored through later stage. Fractures edge

above the CEJ and with a minimum distance of 1 mm are classified as positive and favorable as they can be easily restored in a later stage [21, 10].

SEM was performed using the Inspect S-50 (Thermo Fisher Scientific, Oregon, USA) and fracture details were investigated at a microscale level. In order to accommodate specimens on the microscope stub, teeth crowns were sectioned using the microtome IsoMet (Buehler Ltd, Illinois, USA) at a speed of 60 rpm. Finally, specimens were metallized by applying an ultra-thin coating of electrically conducting metal (Gold) to improve the imaging of samples.

Adhesive fractures occurring at the adhesive interfaces (i.e. composite-dentin and post-composite interfaces) and cohesive fractures (i.e. dentin and composite fractures) were distinguished.

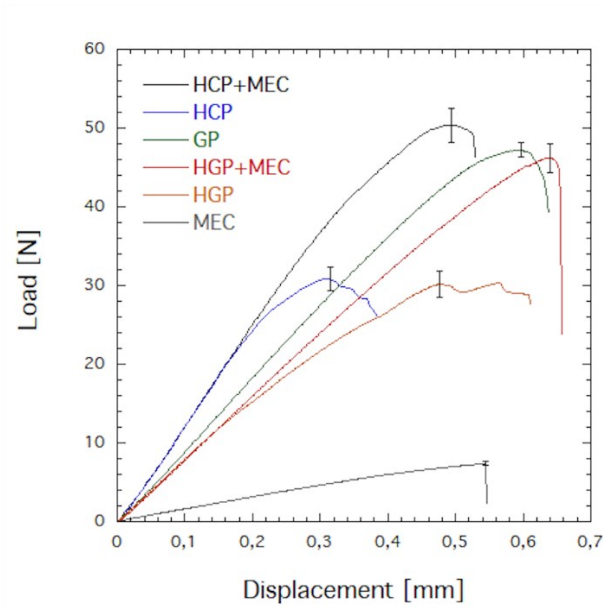
### **3. Results**

Figure 1 reports the mechanical behavior in bending of posts and cements. An initial linear portion detecting the elastic behavior of each composite post and cement can be distinguished. The steepness of each curve in the linear region ( $dP/dy$ ) was computed through the linear best fit and results are reported in table 2. The steepness of MEC is significantly lower ( $p < 0.01$ ) than those of all the other samples, while the steepness of HCP and HCP+MEC is significantly higher ( $p < 0.01$ ) than those detected for all the other samples. However, no significant difference was observed between the steepness of HCP+MEC and HCP, suggesting that the contribution of the composite cement (i.e. MEC) filling the cavity of the hollow carbon fiber post can be neglected. Similarly, no significant difference was found between the steepness of HGP and

HGP+MEC, suggesting that the contribution of the composite cement (i.e. MEC) filling the cavity of the hollow glass fiber post can be neglected. Moreover, this contribution does not allow to reach steepness values typical of compact glass posts (GP), as the steepness of GP is significantly higher ( $p < 0.01$ ) than that of HGP+MEC.

While composite hollow posts filled with cement (i.e. HCP+MEC and HGP+MEC), compact glass post (GC) and the particulate composite cement showed a well-defined break point characterized by a crash fracture, hollow posts (i.e. HCP and HGP) did not show a well defined break point, as these specimens underwent an instability behavior of the mid-span cross section. This instability is shown by the complex load-displacement behavior following the maximum point of HCP and HGP.

The maximum load measured for HCP+MEC ( $50.34 \pm 1.78$  N) was significantly higher than that of HCP ( $31.57 \pm 1.52$  N); the composite cement filling the cavity of the hollow carbon fiber post increased the bending strength of about 59 %. A similar result concerning the reinforcing effect of MEC was observed for the hollow glass fiber post, and an increase of the bending strength of about 51 % was recorded.



**Figure 1.** Results from three-point bending tests: load-displacement curves for hollow carbon fiber post (HCP), hollow glass fiber post (HGP), compact glass fiber post (GP), dual cement Maxcem Elite Chroma (MEC), hollow carbon fiber post filled with Maxcem Elite Chroma cement (HCP+MEC) and hollow glass fiber post filled with Maxcem Elite Chroma cement (HGP+MEC). The bars denote the standard deviation at the maximum load.

Table 2 reports the Young's modulus of HCP, HGP, GP and MEC computed according to equation 1. The rigidity of HCP is significantly higher ( $p < 0.01$ ) than the other endodontic posts. Significantly lower rigidity ( $p < 0.01$ ) were observed for the composite cement.

For HCP, HGP, GP and MEC the axial stiffness is given by the product between the Young's modulus and the first moment of area, these values are reported in Table 2. Similarly, the bending stiffness is given by the product between the Young's modulus and the second moment of area, these values are reported in Table 2.

The axial stiffness and the bending stiffness of hollow fiber reinforced posts filled with cement are computed by adding the contribution to these stiffness of the external shell and internal core (Table 2).

**Table 2.** Geometrical and mechanical properties of endodontic posts and cement. Numbers into brackets denote the standard deviation.

	<b>1<sup>th</sup></b> <b>Moment</b> <b>of Area</b> <b>[mm<sup>2</sup>]</b>	<b>2<sup>nd</sup></b> <b>Moment</b> <b>of Area</b> <b>[mm<sup>4</sup>]</b>	<b>Maximum</b> <b>Load</b> <b>[N]</b>	<b>dP/dy</b> <b>[N/mm]</b>	<b>E</b> <b>[GPa]</b>	<b>Axial</b> <b>Stiffness</b> <b>[kN]</b>	<b>Bending</b> <b>Stiffness</b> <b>[kN·mm<sup>2</sup>]</b>
<b>HCP</b>	0.94	0.0987	31.57 (1.52)	128.05 (2.47)	59.38 (1.14)	55.82 (1.07)	5.86 (0.11)
<b>HGP</b>	0.94	0.0987	30.48 (1.71)	83.67 (2.11)	38.80 (0.98)	36.47 (0.92)	3.83 (0.10)
<b>GP</b>	1.13	0.102	46.45 (0.92)	89.63 (2.13)	40.22 (0.95)	45.44 (1.07)	4.10 (0.10)
<b>MEC</b>	1.00	0.083	7.39 (0.27)	16.63 (1.05)	9.17 (0.58)	9.17 (0.58)	0.76 (0.05)
<b>HGP+MEC</b>	1.13	0.102	46.17 (1.78)	84.37 (3.03)	-	38.27 (0.93)	3.86 (0.11)
<b>HCP+MEC</b>	1.13	0.102	50.34 (2.10)	128.73 (1.91)	-	56.62 (1.08)	5.89 (0.11)

For HGP+MEC, a theoretical steepness of 84.33 N/mm was calculated through the Equation 3, by knowing the Young's moduli of the single components (i.e. the external fiber reinforced shell and the composite core), This value is consistent with the experimental value reported in Table 2 for HGP+MEC. Similarly, a theoretical

steepness of 128.68 N/mm was computed for HCP+MEC, by using Equation 3. This value is consistent with the experimental value reported in Table 2 for HCP+MEC.

Figure 2 reports the mechanical behavior after fatigue cycling for maxillary premolars (Group 1), premolars having an MOD restored with composite (Group 2), and premolars having an MOD cavity restored with the investigated endodontic posts (Groups 3 to 5).

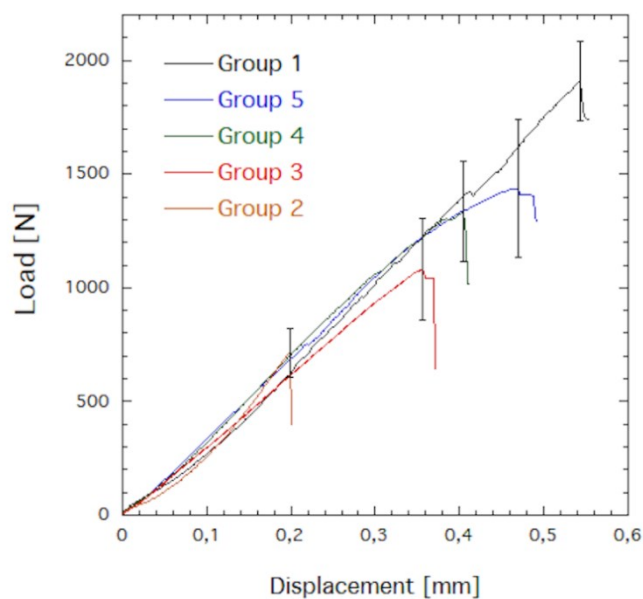


**Figure 2.** Mechanical behavior after fatigue of maxillary premolars (Group 1), premolars having an MOD restored with composite (Group 2), premolars having an MOD cavity restored with GF (Group 3), premolars having an MOD cavity restored with HGP (Group 4), and premolars having an MOD cavity restored with HCP (Group 5).

Table 3 reports the values of mechanical strength for premolars and restored MOD cavities of premolars recorded after fatigue.

**Table 3.** Fracture strength after fatigue of maxillary premolars (Group 1), premolars having an MOD restored with composite (Group 2), premolars having an MOD cavity restored with GF (Group

3), premolars having an MOD cavity restored with HGP (Group 4), and premolars having an MOD cavity restored with HCP (Group 5). Numbers into brackets denote the standard deviation.

	<b>Group 1 – Control</b>	<b>Group 2 – MOD</b>	<b>Group 3 – GP</b>	<b>Group 4 – HGP</b>	<b>Group 5 – HCP</b>
<b>Load [N]</b>	1909 (177)	715 (107)	1083 (224)	1336 (221)	1467 (304)

The strength of sound teeth (Group 1) was significantly higher ( $p < 0.01$ ) than all the other groups. Premolars having an MOD restored with composite (Group 2) showed a mechanical strength significantly lower ( $p < 0.01$ ) than all the other groups. No significant difference was observed in the strength of maxillary premolars restored with the different endodontic posts (Groups 3 to 5).

The failure mode of sound premolars and premolars having an MOD cavity restored with composite or with the different endodontic posts is shown in figure 3.

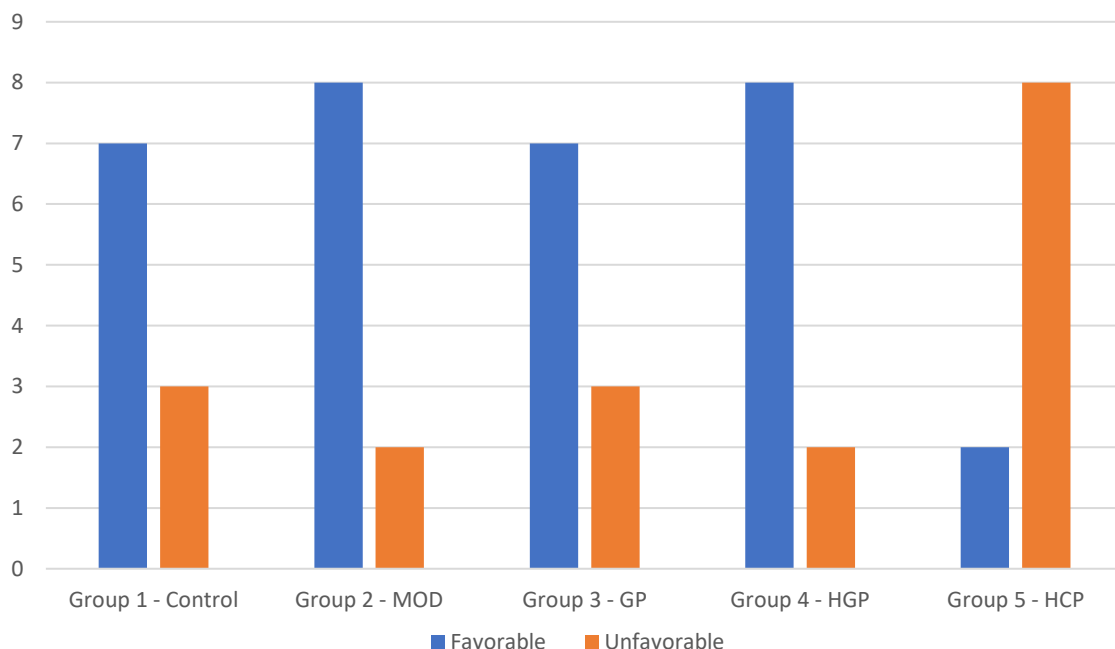


**Figure 3.** Failure mode. Number of teeth for each Group characterized by favorable and unfavorable failure mode.

Fracture patterns of the specimens were evaluated using the digital microscope. Based on the failure mode, fracture types were classified into favorable and unfavorable depending on the position between the CEJ and the fracture surface lower edge (Fig. 4). Fractures edge above the CEJ and with a minimum distance of 1 mm are defined as positive and favorable and can be easily restored subsequently. Besides, fractures below the CEJ that exceed 1 mm distance are defined as negative and unfavorable as they cannot be restored later. MOD cavities restored through composite (Group 2) or through the more compliant glass fiber post (Group 4) showed a favorable type of fracture. Instead, MOD cavities restored through the more rigid carbon fiber post showed unfavorable type of fracture.

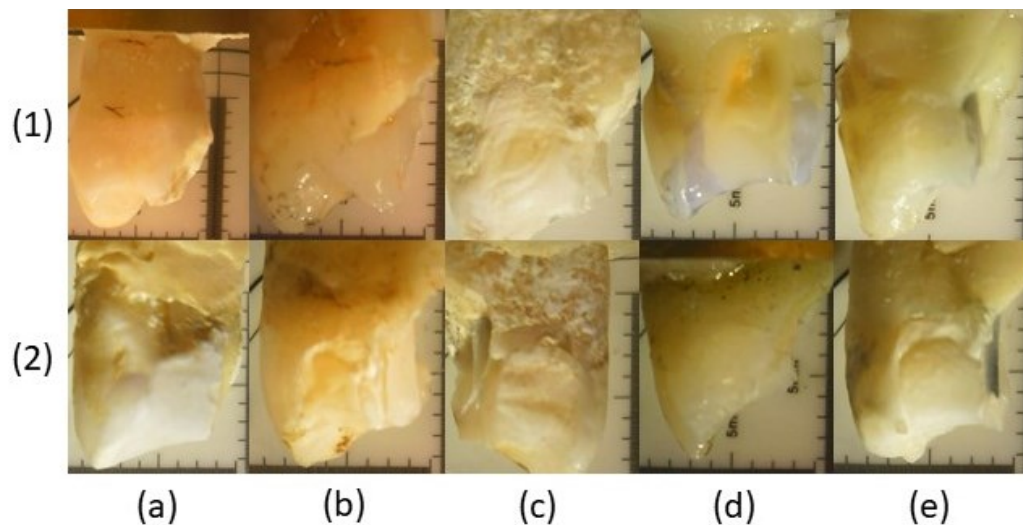


**Figure 4.** Digital microscopy to define 1) favorable and 2) unfavorable fractures of a) control group, b) MOD group, c) glass fiber post group, d) hollow glass fiber post group and e) hollow carbon fiber post group.

High resolution images of the fractured specimens obtained through SEM imaging are reported in Figure 5.

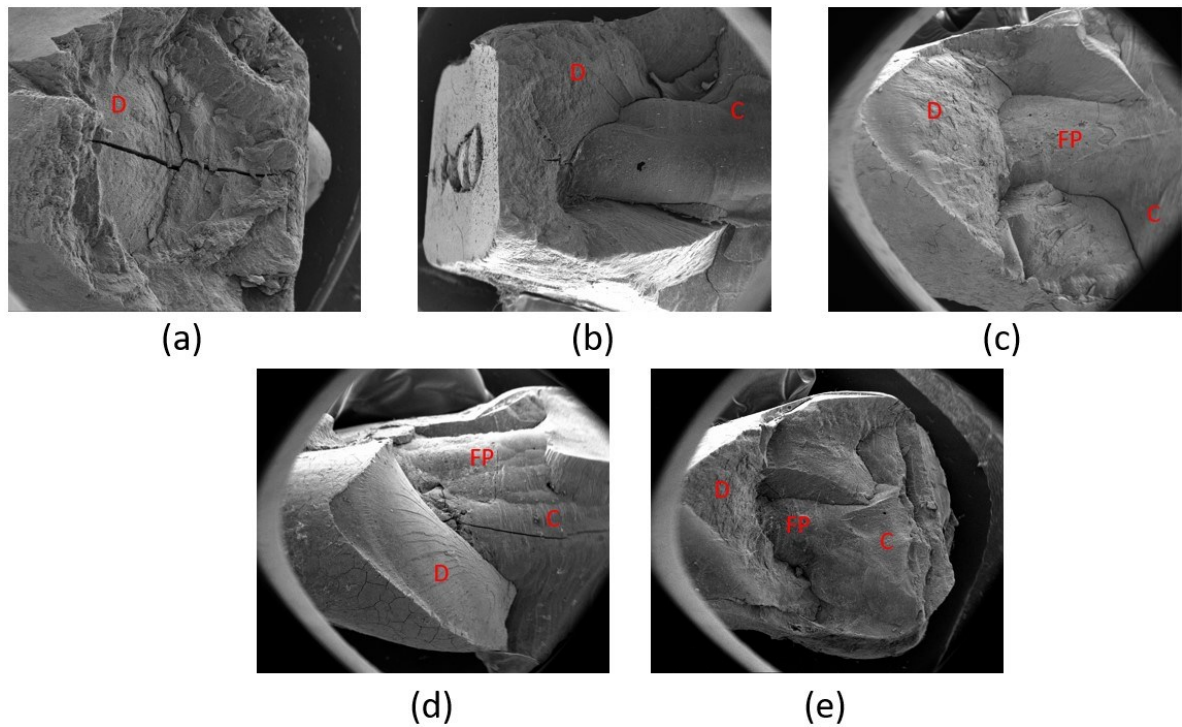


**Figure 5.** Scanning Electron Microscopy (SEM) images of a) control group, b) MOD group, c) glass fiber post group, d) hollow glass fiber post group and e) hollow carbon fiber post group. D=dentine, C=composite, FP=fiber post.

Control group (Group 1) showed a cohesive fracture (Figure 5a) occurring through dentine. Premolars restored with the composite material (Group 2) mainly displayed an adhesive type of fracture (Figure 5b) occurring at the composite-dentine interface propagating through dentine above the CEJ. Teeth restored through fiber posts (Group 3, 4 and 5) showed a mixed type of fracture (Figures 5c, 5d and 5e) involving the adhesive interface between the fiber post and the cement, and a cohesive interface occurring in both the luting cement and dentine.

#### 4. Discussion

In a dental restoration involving composites, materials with different properties and different elastic modulus meet at the adhesive interface layer that is the weaker area of the restoration as debonding is recognised as the main cause of the restorative failure

[22]. Mechanical properties of fiber posts are also relevant for the success of endodontic restorations, since highly rigid endodontic posts transfer the chewing stress apically and stress concentration may lead to restoration failure and root fracture [6]. Continuous fiber reinforced polymers offer the possibility to tailor the stiffness through a material design, and functionally graded composites represent an elegant strategy for designing advanced endodontic posts [23]. Inspired by natural design, the possibility to locate the fiber reinforcement far from the neutral axis represent another strategy for tailoring mechanical properties [24]. This approach allowed to design hollow fiber reinforced endodontic posts recently introduced in the market [15].

Within this study, a variety of fiber posts, including hollow posts, were characterized through the three-point bending test for assessing mechanical properties such as maximum load, elastic modulus, axial and bending stiffness. From the three-point bending results (Figure 1) it is possible to identify an initial linear portion of the load-displacement curve that allows to detect the elastic behavior of the posts and cement. By computing the linear best fit of the curves, the steepness of the linear region ( $dP/dy$ ) is detected and the stiffness of posts and composite cement is calculated (Table 2). In particular, the steepness of carbon fiber posts filled or not with cement (HCP, HCP+MEC) is significantly higher ( $p<0.01$ ) than the other samples. This result can be ascribed to the carbon fiber reinforcement that increases the materials stiffness and allows a more rigid response to the post itself. While the significantly lower values of steepness ( $p<0.01$ ) are achieved by the composite cement (MEC). Observing the results for the steepness of hollow posts filled or not with cement (HCP+MEC, HGP+MEC),

posts filled with cement achieve a higher stiffness but with no significant difference. The Young's modulus measured for GP (Table 2) is consistent with values reported in the literature for glass fiber reinforced endodontic posts [25]. Little is known on the properties of hollow composite endodontic posts, Young's moduli and the steepness of the linear region measured for HGP and HGP+MEC are similar to those recently reported in the literature but some inconsistency can be also observed [15]. This inconsistency can be ascribed to the equations used to compute the Young's modulus and steepness of the linear region, as it is not appropriate to use the equations of compact beams to compute the properties of hollow beams.

Analyzing the load-displacement curves it is worth noting that hollow posts (i.e. HGP and HCP) do not show a well-defined break point. This behavior may be ascribed to mechanical instability. In fact, circular tubes subjected to bending loads are prone to the ovalization of the mid-span cross section. Ovalization evolves till a critical value is reached and from that point the hollow cylinder will buckle [26]. The ovalization of circular tubes is combined with the wrinkling phenomenon, that is the development of short wavelength periodic ripples on the compressive side of the shell. Soon after the wrinkling phenomenon occurs, the circular tube buckles. The load instability limit raises as the shell thickness increases as a direct consequence of the ovalization caused by bending loads [27]. The load-displacement behavior of HGP and HCP as the relative maximum point is reached (Figure 1) suggests that hollow posts are prone to buckling. Figure 2 clearly shows that the mechanical behavior in the elastic region of hollow posts (HGP and HCP) is not affected by the presence of the composite cement

(HGP+MEC and HCP+MEC), and similar stiffness values were recorded between hollow posts and hollow posts filled with cement (Table 2). The composite cement occupies the region of the post close to the neutral axis, therefore its contribution to the post stiffness can be neglected. Instead, in the plastic region of the load-displacement curve (Figure 2), the mechanical behavior of hollow posts filled with the composite cement completely differs from that of hollow posts. The presence of the composite cement in the cavity of hollow posts prevents ovalization and buckling. As a consequence, the strength of HGP+MEC is close to that of GP (Figure 2 and Table 2).

Comparing all the investigated posts, a significantly higher rigidity ( $p < 0.01$ ) were observed for HCP. This result is consistent with the well-known effect of carbon fiber reinforcement that provides stiffness higher than other types of reinforcement (e.g. glass fibers).

Fracture strength of teeth after fatigue was evaluated by analyzing the maximum load achieved by the specimens. Control group (Group 1) achieved a significantly higher strength ( $p < 0.01$ ) than other groups, while a significantly lower strength ( $p < 0.01$ ) was attained for the MOD group. No significant difference was found between teeth restored with different types of posts.

Failure mode is strictly related to the axial stiffness of the post itself. An endodontic post with a high axial stiffness transfers the higher stress at the root canal walls, thus promoting an unfavorable fracture under the cement-enamel junction. This type fracture does not allow to repair and reconstruct the tooth if failure occurs. In the current research, the higher axial stiffness was achieved by the hollow carbon post

presenting the higher percentage of unfavorable fractures (80% of the specimens). Besides, fiber posts with a lower axial stiffness allows to obtain a lower stress concentration at the root canal walls and promoting a more uniform stress distribution to the coronal dentin. These posts lead to a favorable fracture that can be often repaired. Hollow glass posts that present a significantly lower axial stiffness than other posts leads to a high percentage of favorable fractures (80% of the specimens). On the other hand, the compact glass post that has a higher axial stiffness than the hollow one, achieves a 70% of favorable fractures (Figures 3 and 4). A cohesive type of fracture occurring through dentine (Figure 5a) was observed in the control group (Group 1), while an adhesive type of fracture occurring at the composite-dentine interface was found for premolars restored through the composite material (Group 2). It is worth noting that teeth restored through fiber posts (Group 3, 4 and 5) showed a mixed type of fracture (Figures 5c, 5d and 5e) involving the adhesive interface between the fiber post and the cement as well as a cohesive interface occurring in both the luting cement and dentine.

## **5. Conclusions**

The strength of premolars having an MOD cavity restored through particulate composite material is significantly lower than that of a sound tooth. The use of continuous fiber reinforced posts significantly increases the strength of teeth having an MOD cavity. Although carbon fiber reinforced posts retain the maximum strength among the investigated post and core restorations, they also lead to an unfavorable type of fracture. Instead, the more compliant glass fiber reinforced posts allows to restore

MOD cavity providing a strength close to that of carbon fiber post, but the type of fracture is more favorable, thus allowing for a further tooth re-treatment in the case of tooth failure.

## References

1. European Society of Endodontology. Quality guidelines for endodontic treatment: consensus report of the European Society of Endodontology. *International endodontic journal*. 2006; 39(12), 921-930;
2. Qing H.; Zhu Z.; Chao Y.; Zhang W. In vitro evaluation of the fracture resistance of anterior endodontically treated teeth restored with glass fiber and zircon posts. *J Prosthet Dent*. 2007; 97(2):93-8.
3. Mergulhão V.A.; de Mendonça L.S.; de Albuquerque M.S.; Braz R. Fracture Resistance of Endodontically Treated Maxillary Premolars Restored With Different Methods. *Oper Dent*. 2019; 44(1):E1-E11.
4. Sasaki K.; Yamamoto T.; Ikawa T.; Shigeta Y.; Shigemoto S.; Ando E.; Ogawa T.; Ihara K. Pre-endodontic Post and Core Technique for Endodontic and Prosthodontic Treatment. *J Contemp Dent Pract*. 2018; 19(1):117-122.
5. Tsintsadze N.; Garcia M.; Grandini S.; Goracci C.; Ferrari M. Effect of Reciprocal endodontic treatment with three different post space preparation instruments on fiber post retention. *Am J Dent*. 2015; 28(5):251-4.
6. De Santis R.; Prisco D.; Apicella A.; Ambrosio L.; Rengo S.; & Nicolais L. Carbon fiber post adhesion to resin luting cement in the restoration of endodontically treated teeth. *Journal of Materials Science: Materials in Medicine*. 2000; 11(4), 201-206.

7. Prisco D.; De Santis R.; Mollica F.; Ambrosio L.; Rengo S.; Nicolais L. Fiber post adhesion to resin luting cements in the restoration of endodontically-treated teeth. *Operative Dentistry-University of Washington*. 2003; 28(5), 515-521.
8. Maietta S.; De Santis R.; Catauro M.; Martorelli M.; Gloria A. Theoretical design of multilayer dental posts using CAD-based approach and sol-gel chemistry. *Materials*. 2018; 11(5), 738
9. Gbadebo OS.; Ajayi DM.; Oyekunle, O.O.; Shaba, P.O. Randomized clinical study comparing metallic and glass fiber post in restoration of endodontically treated teeth. *Indian J Dent Res*. 2014; 25(1):58-63.
10. Alkhatri, R.; Saleh, A. R. M.; Kheder, W. Impact of post and core materials on the apical extension of root fracture in root canal treated teeth. *Journal of Materials Research and Technology*. 2021, 10, 730-737.
11. De Santis, R.; Russo, T.; Gloria, A. An analysis on the potential of diode-pumped solid-state lasers for dental materials. *Materials Science and Engineering: C*. 2018, 92, 862-867.
12. Özlek, E.; Neelakantan, P.; Matinlinna, J.P.; Belli, S.; Ugur, M.; Kavut, I. Adhesion of Two New Glass Fiber Post Systems Cemented with Self-Adhesive Resin Cements. *Dent J (Basel)*. 2019; 7(3):80. doi: 10.3390/dj7030080.
13. Plotino, G.; Grande, N.M.; Isufi, A.; Ioppolo, P.; Pedullà, E.; Bedini, R.; Gambarini, G.; Testarelli, L. Fracture Strength of Endodontically Treated Teeth with Different Access Cavity Designs. *J Endod*. 2017, 43(6):995-1000. doi: 10.1016/j.joen.2017.01.022.

14. Sarkis-Onofre, R.; Jacinto, R.C.; Boscato, N.; Cenci, M.S.; Pereira-Cenci, T. Cast metal vs. glass fibre posts: a randomized controlled trial with up to 3 years of follow up. *J Dent.* 2014, 42(5):582-7. doi: 10.1016/j.jdent.2014.02.003.
15. Lo Giudice, G., Ferrari Cagidiaco, E., Lo Giudice, R., Puleio, F., Nicita, F., & Calapaj, M. (2019). Evaluation of mechanical properties of a hollow endodontic post by three point test and SEM analysis: A pilot study. *Materials*, 12(12), 1983.
16. Figueiredo, F.E.; Martins-Filho, P.R.; Faria-E-Silva, A.L. Do metal post-retained restorations result in more root fractures than fiber post-retained restorations? A systematic review and meta-analysis. *J Endod.* 2015, 41(3):309-16. doi: 10.1016/j.joen.2014.10.006.
17. Doshi, P.; Kanaparthi, A.; Kanaparthi, R.; Parikh, D.S. A Comparative Analysis of Fracture Resistance and Mode of Failure of Endodontically Treated Teeth Restored Using Different Fiber Posts: An In Vitro Study. *J Contemp Dent Pract.* 2019, 20(10):1195-1199.
18. Özyürek, T.; Topkara, C.; Koçak, İ.; Yılmaz, K.; Gündoğar, M.; Uslu, G. Fracture strength of endodontically treated teeth restored with different fiber post and core systems. *Odontology.* 2020, (4):588-595. doi: 10.1007/s10266-020-00481-4.
19. De Santis, R.; Gloria, A.; Maietta, S.; Martorelli, M.; De Luca, A.; Spagnuolo, G.; Rengo, S. Mechanical and thermal properties of dental composites cured with CAD/CAM assisted solid-state laser. *Materials.* 2018, 11(4), 504.
20. De Santis, R.; Lodato, V.; Gallicchio, V.; Prisco, D.; Riccitiello, F.; Rengo, S.; Rengo, C. Cuspal Deflection and Temperature Rise of MOD Cavities Restored

through the Bulk-Fill and Incremental Layering Techniques Using Flowable and Packable Bulk-Fill Composites. *Materials*. 2020, 13, 5664.

21. Padmanabhan, P. A comparative evaluation of the fracture resistance of three different pre-fabricated posts in endodontically treated teeth: An in vitro study. *Journal of conservative dentistry*. 2010, 13(3), 124.
22. De Santis, R.; Mollica, F.; Prisco, D.; Rengo, S.; Ambrosio, L.; Nicolais, L. A 3D analysis of mechanically stressed dentin–adhesive–composite interfaces using X-ray micro-CT. *Biomaterials*. 2005, 26(3), 257-270.
23. Fujihara, K.; Teo, K.; Gopal, R.; Loh, P. L.; Ganesh, V. K.; Ramakrishna, S.; Chew, C. L. Fibrous composite materials in dentistry and orthopaedics: review and applications. *Composites Science and Technology*. 2004, 64(6), 775-788.
24. De Santis, R.; Sarracino, F.; Mollica, F.; Netti, P. A.; Ambrosio, L.; Nicolais, L. Continuous fibre reinforced polymers as connective tissue replacement. *Composites science and technology*. 2004, 64(6), 861-871.
25. Stewardson, D. A.; Shortall, A. C.; Marquis, P. M.; Lumley, P. J. The flexural properties of endodontic post materials. *dental materials*. 2010, 26(8), 730-736.
26. Lee, K. L.; Pan, W. F.; Kuo, J. N. The influence of the diameter-to-thickness ratio on the stability of circular tubes under cyclic bending. *International Journal of Solids and Structures*. 2001, 38(14), 2401-2413.
27. Kyriakides, S.; Ju, G.T. Bifurcation and localization instabilities in cylindrical shells under bending—I. Experiments. 1992, 29(9), 1117–1142.

## **Chapter 4**

### **Cusps deflection and temperature rise of MOD cavities restored through the bulk-fill and the incremental layering techniques using flowable and packable bulk-fill composites**

#### **1. Introduction**

In the last decades composite materials have been widely used for conservative dentistry, although resin based composites are subjected to volumetric contraction during polymerization, they provide satisfactory aesthetics [1]. Due to this contraction, a shrinkage stress can cause an adhesive debonding at the tooth-adhesive-composite interfaces [2, 3]. Bacterial leakage, dentinal sensibility and secondary caries are the clinical effects of interfacial microleakage [4, 5]. Many techniques have been developed in order to reduce the stress at the adhesive interface. The incremental restoration technique, in direct restorations, has been developed to vary the shrinkage pattern [6]. This technique is based on filling the tooth cavity with micro-hybrid or nanohybrid conventional composite resin increments. On the other hand, the incremental technique increases both the clinical chair time required for dental reconstruction and technique sensitivity [7, 8].

The high translucency and a powerful initiator system confer to bulk-fill resin composites a high depth of cure [1, 9, 10]. Compared to traditional incremental filling techniques, cavities with a depth higher than 4 mm can be filled through the bulk-fill technique, thus reducing the chair time to fill a cavity [7,11]. Depending on rheological

properties, bulk-fill RBCs can be classified in flowable and packable [12]. Flowable composites are low viscosity RBCs directly injected into the cavity through a needle with the advantage of a self-adaption to the cavity walls. One of the first flowable bulk-fill material on the market is represented by Smart Dentin Replacement – SDR (Sirona Dentsply, Konstanz, Germany) bulk-fill composite. However, capping with a conventional composite material is recommended to avoid wear [8, 13, 14].

Instead, high viscosity bulk-fill RBCs show mechanical properties similar to conventional nanohybrid and microhybrid composite materials. The application of these high-viscosity materials into the cavity is achieved through a traditional spatula or through a sonic vibration handpiece to reduce viscosity while injecting materials such as SonicFill 2 – SFL (Kerr Corporation, Orange, California) [1, 9]. Due to the high percentage of resin matrix, bulk-fill flowable RBCs should achieve a high shrinkage. Several studies have demonstrated that the lower shrinkage is achieved at the bottom of the cavity, because the light cure intensity decreases as the curing depth increases, thus generating a polymerization degree gradient through the composite [15, 16, 17]. Compared to other bulk-fill resin composites for posterior teeth restoration, SonicFill 2 shows higher inorganic filler amount [18]. Mechanical properties of SDR are higher than other flowable RBCs but lower than those of regular nanohybrid or microhybrid RBCs, as a consequence SDR shows higher plastic deformation and creep than other low-viscosity RBCs [8]. For this reason clinicians recommend capping with 2 mm occlusal increment using conventional high viscosity composite [19]. It is reported that SonicFill 2 contracts less than SDR, and the volumetric shrinkage values

compared with other flowable materials are significantly different. The different amount of organic matrix in the material has a direct relationship with the shrinkage values. SonicFill 2 is a composite material with a very high filler content and thus it is expected to have a lower shrinkage value than a flowable material which has a higher resin content. SonicFill 2 achieves the properties of a hybrid material after polymerization, but it has the consistency similar to that of a flowable material when it is placed through a sonic vibration handpiece. SDR has a higher volumetric shrinkage, but stress can be lower than Sonicfill 2. This can be attributed to the new modulator that slows the polymerization rate, reducing the stress [20]. The difference in volumetric shrinkage, due to the viscosity of the material, is demonstrated by Kim et al. The study proves that a higher shrinkage and a lower modulus is achieved by a low-viscosity composite (e.g. SDR) compared to a high-viscosity composite (e.g. SonicFill 2) [1, 19]. Sung-Ae et al. showed that bulk-fill composites with low filler content have a higher polymerization shrinkage than those with high filler content [21]. An important aspect related to the filler content is the elastic modulus of the composite material. Ilie et al. tested the mechanical properties of different resin-based composite materials. The study resulted in the variation of the elastic modulus due to a variation of the filler content. In particular, SonicFill 2 has a filler loading higher than SDR, thus achieving a significantly higher value of the elastic modulus [8]. This result is in accordance with other studies in which SonicFill 2 achieves significantly greater values of flexural and compressive strength compared to SDR, thanks to the filler loading

[22]. Other studies demonstrate that SDR has a lower flexural and compressive strength compared with other bulk-fill composites [23].

Clinically, a main concern of bulk-fill RBCs is a potentially increased shrinkage stress developing at the composite-tooth walls interface, and also temperature rise occurring for the polymerization of massive amount of composite material. Polymerization shrinkage can be directly evaluated through volumetric or linear measurements, based on 3D imaging or displacement transducers, respectively [24 - 27]. From a clinical point of view, an accurate method to evaluate the effects of composite shrinkage on dental tissues is the cuspal displacement measurement, with the inter-cusps distance as length variation measurement. It is reported that teeth with small cavities deform less than those with large cavities, and the intercuspal distance decreases significantly in the first 60 min after starting curing. A gradual recovery of the cusps toward the original dimensions over a longer period has also been suggested [28]. Fleming et al. measured cusps distance variation by measuring the buccal and lingual cusps deflection of the extracted teeth through a twin displacement gauge sensor, and restoration was achieved through an incremental technique with eight increments. The filling technique minimized cuspal deflection by constraining the cusps, resulting in an under-estimation of the deflection expected when one cusp was not constrained [29]. Kwaon et al. measured cusps deflection through LVDT probes using bulk-fill and incremental techniques. The incremental filling technique yielded significantly lower cuspal deflection than the bulk filling technique [6]. A microscope with a micrometer stage was used by Alomari et al. to measure the distance between

the cusp tips. The study resulted in high values of the cusps deflection, with a maximum deflection of 47  $\mu\text{m}$  and a minimum of 23  $\mu\text{m}$ . These high values have been ascribed to the strong bonding between the restoration and the cavity walls. A subsequent water immersion of the samples for 24 hours resulted in a cusp relaxation between 12  $\mu\text{m}$  and 17  $\mu\text{m}$  [30].

Little is known on cusps deflection as bulk-fill composites are used for restoring mesio-occlusal-distal (MOD) cavities of premolars according to the incremental or to the bulk-fill techniques. Kim et al. evaluated cusp deflection of aluminium teeth according to a variety of bulk-fill composites considering both the incremental and the bulk-fill techniques [31]. The aim of this investigation is to evaluate cuspal deformation during restoration of MOD cavities of human premolars by using both the bulk-fill and the incremental layering techniques using two bulk-fill composite materials largely differing in viscosity.

The null hypothesis is that different layering techniques and different types of composite materials would affect the cusps distance variation and temperature rise.

## **2. Materials and Methods**

Two bulk-fill RBCs largely differing in material composition and rheological properties have been tested. SDR flow+ is one component, light cured, radiopaque, flowable resin composite. SDR is available in pre-dosed (0.25 g) compula tips for intraoral application. Sonicfill 2 is a packable composite applied through a vibration handpiece, providing the sonic-activated dispensation of the composite material, thus reducing viscosity during placement [9].

Viscosity of SDR is expected to be similar to that of flowable restorative composites (viscosity lower than 1 kPa·s), while viscosity of SFL is expected to be similar to that of highly filled RBCs (viscosity higher than 100 kPa·s) [12]. Table 1 depicts materials composition of the two bulk-fill RBCs and restoration techniques, and the initiator system of both composites is based on camphorquinone.

**Table 1.** Composite materials composition and restoration techniques.

<b>Material</b>	<b>Manufacturer</b>	<b>Composition</b>	<b>Restorative Technique</b>	<b>Acronym</b>
<b>SonicFill 2</b>	Kerr, USA	Matrix: Bis-GMA, TEGDMA, EBPDMA Filler 83.5wt%: SiO <sub>2</sub> , glass, oxide	Bulk	SFLB
			Incremental	SFLI
<b>SDR flow +</b>	Sirona Dentsply, USA	Matrix: UDMA, TEGDMA, EBPDMA Filler 68wt%: Ba-Al-F-B-Si glass and St-Al-F-Si glass	Bulk	SDRB
			Incremental	SDRI

Linear shrinkage (Figure 1a) of SFL and SDR bulk composites was investigated up to 3600 s through a protocol previously described [3]. Briefly, bulk composites were injected into prismatic PTFE moulds of 5.0mm×5.0mm×1.5mm. A Mylar strip was used to handle the composite and to position each specimen between the mechanical arms of an Instron extensometer 2620-601 (Instron Ltd., High Wycombe, United Kingdom). Shrinkage measurements were evaluated in the direction perpendicular to the light curing front. A filtered photocell obtained from Demetron LED radiometer (Kerr Corporation) was employed to monitor light power level. The light curing unit

Swiss Master Light (EMS, Nyon, Switzerland) at an intensity level of 1000 mW/cm<sup>2</sup> and exposure time of 10 s was used to light cure composite materials. Light power and linear shrinkage data were simultaneously acquired at a speed of 50 p/s up to 3600 s using the National Instrument DAC (National Instruments, Austin, Texas) driven by Signal Express software (National Instruments). Five specimens for each bulk fill composite were used and data at 300 s and 3600 s were analysed using two-way ANOVA followed by Tukey's test at a critical value of 0.05.

Mechanical properties of SFL and SDR bulk-fill composites were investigated through compression tests (Figure 1b). Bulk-fill composites were injected into prismatic PTFE moulds containing a cylindrical cavity having a 3 mm diameter and a 4 mm height. Mylar strip placed in the bottom and in the up side of the cylindrical PTFE cavity were used to prevent material flow and oxidation of the composite material during the light curing process. The light curing unit Swiss Master Light (EMS) at an intensity level of 1000 mW/ cm<sup>2</sup> and exposure time of 20 s was used to light cure composite materials. Specimens were kept in a dark environment at room temperature for 48 h before mechanical testing. An Instron 5566 (Instron Ltd.) testing machine, equipped with a 5 kN load cell, was employed for compression tests at a speed of 1 mm/min. The experimentally measured dynamometer compliance was  $4.18 \cdot 10^{-5}$  mm/N, and this value was considered to determine the true deformation of short specimens in compression. Mechanical strength was evaluated by considering the ratio of the maximum applied force and the cross-section area of the specimen, strain to failure was calculated as the ratio of the maximum displacement and the specimen

height, while Young's modulus in compression was evaluated through the steepness of the stress-strain curve in the elastic region. Compression tests were performed within one hour ( $t_0$ ) or 72 h ( $t_{72h}$ ) from polymerization. Five replicates for each composite and for each time-point were used. Data were analysed using two-way ANOVA followed by Tukey's test at a critical value of 0.05.

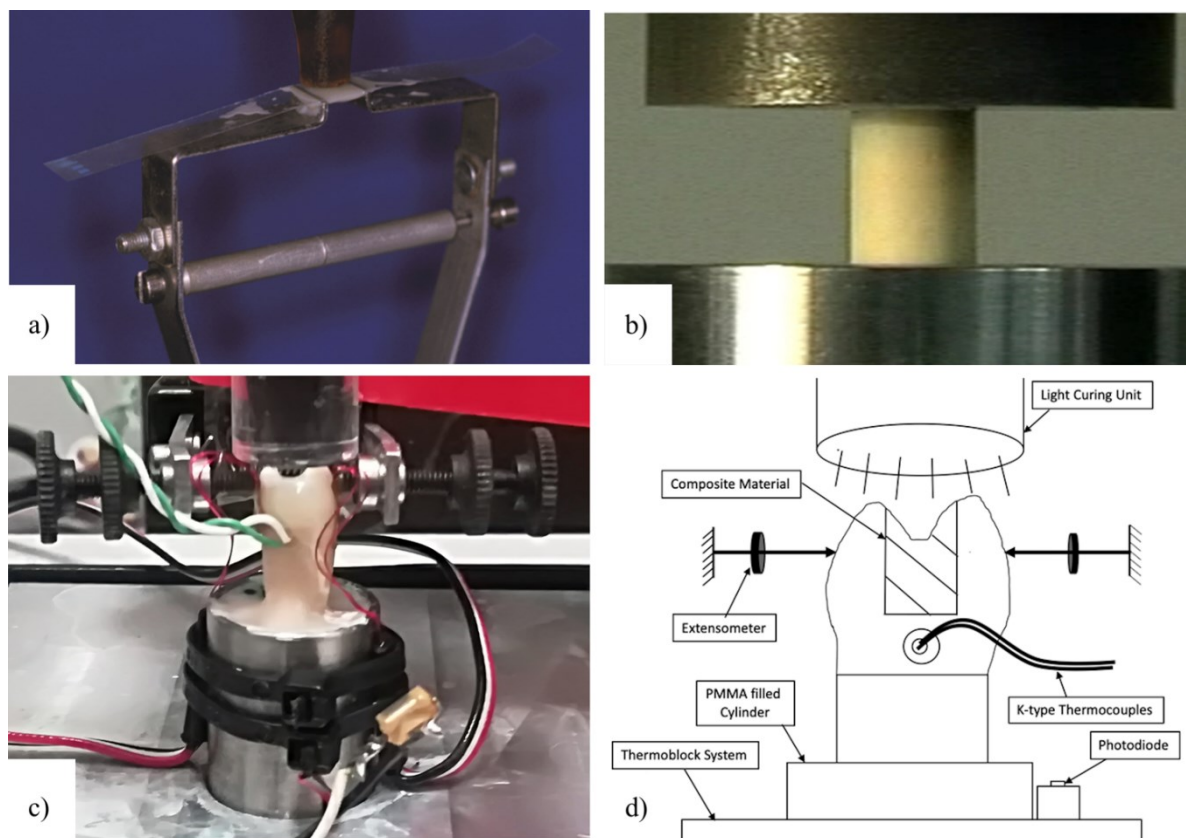


**Figure 1.** (a) Linear shrinkage evaluated in the direction perpendicular to the light curing front; (b) compression test of cylindrical specimens with diameter of 3 mm and height of 4 mm; (c) set-up adopted for the simultaneous measurement of cusps distance, temperature and light intensity; (d) description of the elements involved for the simultaneous measurement of cusps distance, temperature and light power.

A total of forty extracted upper premolars for orthodontic treatments were assigned to this study approved by the Ethics Committee of the University of Naples Federico

II, with protocol number 137 2017. Before testing, caries and defects free premolars were selected. They were sterilized with HClO 2.5 % solution, then stored in distilled water until testing. Teeth were selected according to an average length of  $22 \pm 1$  mm, a buccal-lingual dimension of  $7 \pm 1$  mm and a disto-mesial distance of  $9 \pm 1$  mm. Teeth dimensions were measured with a digital caliper (Mitutoyo, Takatsuku, Japan). Teeth were fixed in a cylindrical metal mold of 16mm diameter using acrylic resin. Each tooth was X-ray scanned with the Partner 70 equipment (Anthos, Bologna, Italy) in the mesial- distal projection, bucco-lingual and occlusal-apical at 70 kV for 0.08 seconds. Dental radiographs were processed with the MicroDicom viewer v3.0.1 software (MicroDicom, Sofia, Bulgaria).

Standardized MOD cavities were prepared in each premolar with a 4 mm cavity depth and 3mm intercuspidal width. Cavities were obtained through a diamond bur mounted on the turbine Fona8080 (Fonadental, Assago, Italy) on a high-speed contra-angle. Dimensions of each cavity preparation were measured using the digital caliper. Buccal and palatal walls of each cavity were prepared parallel to each other.

Teeth cusps and restorations MOD cavities dimensions are reported in Table 2.

**Table 2.** Teeth cusps and restorations MOD cavities mean dimensions expressed in mm.

Numbers in brackets represent the standard deviation.

	MOD Thickness	MOD Height	MOD Width	Vestibular Cusp Height	Lingual Cusp Height	Vestibular Cusp Width	Lingual Cusp Width	Vestibular Cusp Thickness	Lingual Cusp Thickness
<b>SFLB</b>	3.05 (0.65)	4.07 (0.20)	6.67 (0.28)	6.48 (0.81)	5.88 (1.02)	7.1 (0.31)	6.21 (0.31)	3.16 (0.10)	3.06 (0.35)

<b>SFLI</b>	2.85 (0.57)	3.96 (0.43)	6.51 (0.39)	6.67 (0.72)	5.59 (0.86)	6.88 (0.25)	6.14 (0.64)	3.41 (0.31)	3.35 (0.42)
<b>SDRB</b>	2.96 (0.48)	3.83 (0.56)	6.44 (0.21)	6.05 (0.53)	5.57 (1.1)	6.64 (0.50)	6.20 (0.08)	3.15 (0.33)	2.71 (0.40)
<b>SDRI</b>	3.29 (0.17)	4.01 (0.61)	6.60 (0.12)	5.97 (0.59)	5.36 (0.82)	6.9 (0.11)	6.26 (0.13)	3.02 (0.42)	2.90 (0.39)

Teeth were randomly divided into two groups (SDR and SFL). Samples of Group SDR were restored with SDR flow + (Sirona Dentsply) composite, while samples of Group SFL were restored with SonicFill 2 (Kerr Corporation) composite. Each group was then divided into two subgroups (SFLB, SFLI and SDRB, SDRI) according to the restorative technique (Table 1). Groups SFLB and SDRB were restored using the bulk-fill technique (4mm thickness), groups SFLI and SDRI were restored through the incremental technique (two increments, 2mm each).

After cavity preparation, teeth were subjected to an adhesive procedure: acid etching (enamel and dentine etching for 30 s and 15 s, respectively) using 37% phosphoric acid (Gerhò, Bolzano, Italy); rinsing and drying for 5 seconds; application of the adhesive system Optibond SE (Kerr Corporation) and photo-polymerization with the Swiss Master Light (EMS) curing unit at an intensity of 1000 mW/cm<sup>2</sup>. SDR flow + was injected into the cavity using a specific manual gun. SonicFill was dispensed directly into dental cavities using the Sonicfill handpiece.

Premolars were cemented in aluminium cylinders (D=16 mm) using a low temperature self-curing acrylic resin. Each sample was heated at 35 °C through a

ThermoBlock system (Falc, Genova, Italy), and its temperature was kept constant during the test (Figure 1c and 1d).

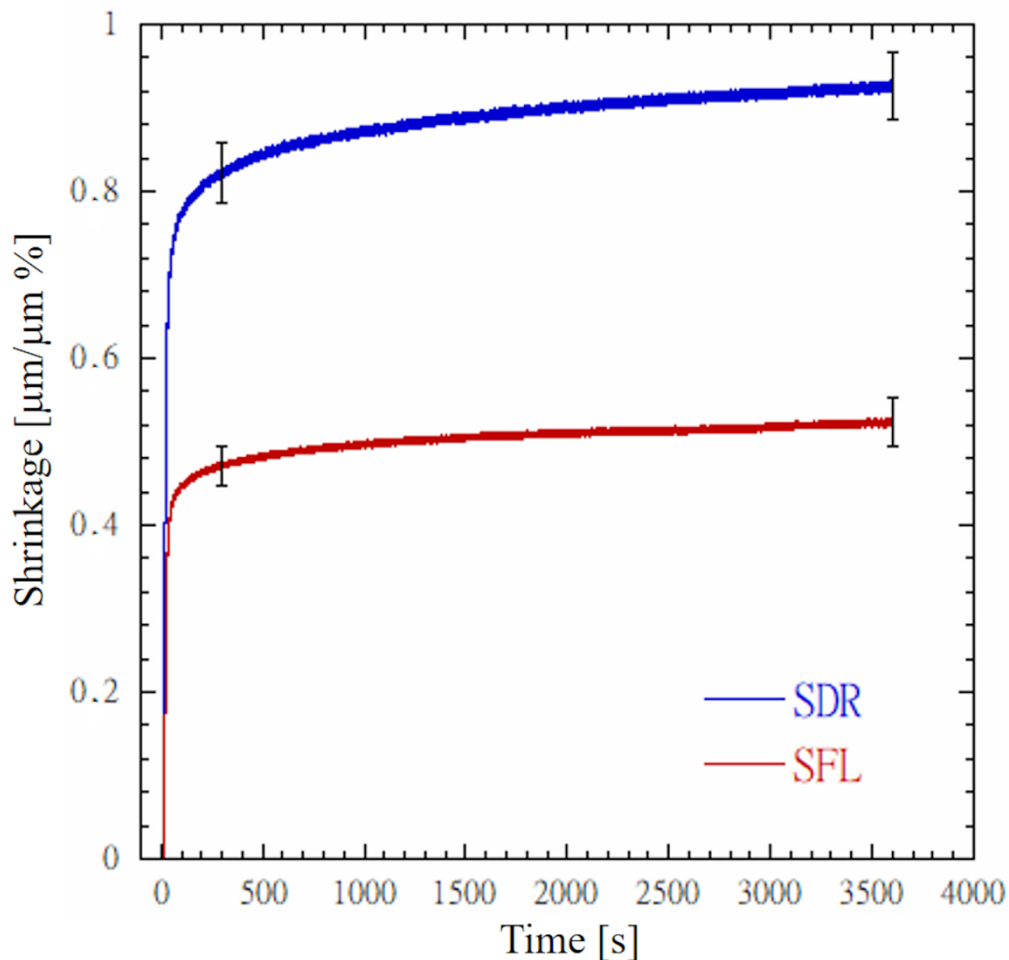
The Instron Extensometer A1439-1014 (Instron Ltd.) was used to measure the variation of the distance between cusps during photopolymerization and during the dark reaction phase up to 3600 s. A filtered photocell, obtained from Demetron LED radiometer (Kerr Corporation), was employed to monitor light power level. Disposable K-type thermocouples (RS components, Corby, United Kingdom), placed into a standardized hole created 1 mm below the cavity floor (Figure 1d), were used to measure temperature variation. The light curing unit Swiss Master Light (EMS) at an intensity level of 1000 mW/cm<sup>2</sup> and exposure time of 20 s was employed to cure bulk fill composites. Before each test, the PM100D ThorLab energy meter console (ThorLabs, Newton, New Jersey), equipped with a S121C sensor (ThorLabs) and connected to the PMD100D software running under LabView (National Instruments), was employed to measure power output of the light curing unit.

Cusps distance, temperature and light power data were simultaneously acquired at a speed of 50 p/s up to 3600 s using the National Instrument DAC (National Instruments) driven by Signal Express software (National Instruments).

Five specimens for each bulk fill composite and for each restorative technique (Table 1) were used, and data at 300 s and 3600 s were analysed using two-way ANOVA followed by Tukey's test at a critical value of 0.05.

### **3. Results**

Figure 2 depicts typical shrinkage profiles recorded for SDR and SFL. A steep shrinkage profile can be observed for both composites as the light is turned on. After 300 s the mean shrinkage value of SFL is significantly lower ( $p < 0.05$ ) than that of SDR. Mean shrinkage values for SDR and SFL are  $0.822 \pm 0.037 \mu\text{m}/\mu\text{m}\%$  and  $0.471 \pm 0.023 \mu\text{m}/\mu\text{m}\%$ , respectively. As expected, shrinkage continues to increase during the dark reaction phase, and at 3600 s its values are significantly higher ( $p < 0.05$ ) than those reported at 300 s. The mean shrinkage values at 3600 s for SDR and SFL are  $0.925 \pm 0.041 \mu\text{m}/\mu\text{m}\%$  and  $0.523 \pm 0.029 \mu\text{m}/\mu\text{m}\%$ , respectively.



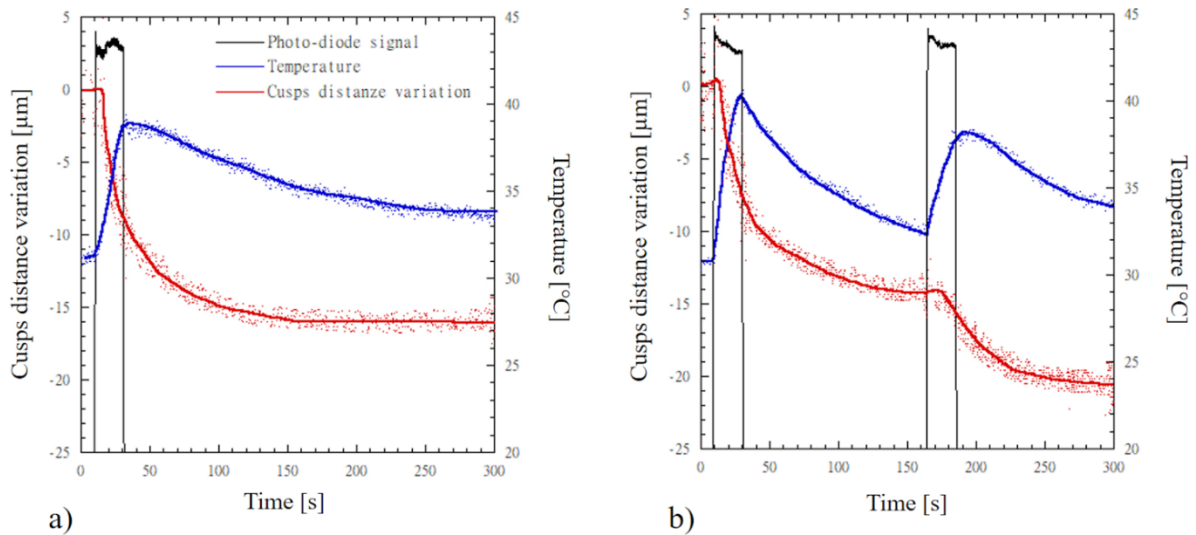
**Figure 2.** Shrinkage profiles recorded for SDR and SDR bulk fill composites

Table 3 reports mechanical properties measured in compression for SDR and SFL bulk fill composites. At both time points, SFL shows a compressive strength ( $\sigma$ ) significantly higher ( $p < 0.05$ ) than those recorded for SDR. At both time points, also the Young's modulus (E) of SFL is significantly higher ( $p < 0.05$ ) than those recorded for SDR. Instead, at both time points, strain to failure ( $\epsilon$ ) of SFL is significantly lower ( $p < 0.05$ ) than those measured for SDR. The difference in mechanical properties of the two bulk fill composites suggests that SFL is stiffer than SDR, but SDR is more compliant than SFL.

**Table 3.** Mechanical properties measured in compression for the SDR and SFL bulk fill composites.  $\sigma$ ,  $\epsilon$  and E represent the compressive strength, the strain to failure and the Young's modulus, respectively. Numbers in brackets represent the standard deviation.

Bulk fill Composite	Time t0			Time 72h		
	$\sigma$ [MPa]	$\epsilon$ [%]	E [GPa]	$\sigma$ [MPa]	$\epsilon$ [%]	E [GPa]
SDR	234 (13)	19.4 (0.3)	1.7 (0.1)	277 (10)	16.7 (0.3)	3.1 (0.1)
SFL	297 (18)	6.4 (0.4)	5.1 (0.2)	329 (36)	5.9 (0.5)	8.5 (0.4)

Simultaneous time measurements of cusps distance variation, temperature and photo-diode signal for MOD cavities restored with SonicFill 2 are reported in figure 3. The photo-diode signal is reported in an arbitrary scale and it is used to detect the light curing and the dark reaction phases. For both the bulk fill (Fig. 3a) and incremental (Fig. 3b) techniques, a delay is observed in the cusps distance variation before a steep contraction occurs.



**Figure 3.** Simultaneous time measurements of cusps distance variation, temperature and photo-diode signal for MOD cavities restored with SonicFill 2. The photo-diode signal is reported in an arbitrary scale and it is used to detect the light curing and the dark reaction phases. MOD cavities restored according to: a) the bulk-fill technique; b) the incremental technique.

A steep cusps distance variation is observed for both the bulk fill and incremental techniques during the light curing phase, and cusps distance variation still occurs at a lower steepness through the dark reaction phase (Fig. 3). For the incremental technique, a further step cusps distance variation is observed as the second composite layer undergoes polymerization. Mean values of cusps distance variation of MOD cavities restored with SonicFill 2 have been computed after 300 s and 3600 s (Table 4).

**Table 4.** Cusps distance variation at 300s and at 3600s.

	300s		3600s	
<b>Material</b>	<b>Mean value</b> <b>(Std. deviation)</b> <b>(<math>\mu\text{m}</math>)</b>	<b>P</b> <b>value</b>	<b>Mean value</b> <b>(Std. deviation)</b> <b>(<math>\mu\text{m}</math>)</b>	<b>P value</b>

<b>SFLB</b>	16.3 (5.6)	0.95	22.9 (9.2)	0.89
<b>SFLI</b>	20.2 (5.5)		27.5 (7.2)	
<b>SDRB</b>	11.8 (3.0)	0.12	20.8 (3.5)	0.43
<b>SDRI</b>	21.8 (1.9)		28.3 (5.0)	

Cusps distance variation measured for tooth restored through the incremental technique ( $20.2 \pm 5.5 \mu\text{m}$ ) is higher than that measured for tooth restored through the bulk fill technique ( $16.3 \pm 5.6 \mu\text{m}$ ), however the difference between the means is not statistically significant ( $p = 0.946$ ). Temperature rise observed for SFLB and SFLI are  $8.2 \text{ }^\circ\text{C} \pm 1.6 \text{ }^\circ\text{C}$  and  $9.5 \text{ }^\circ\text{C} \pm 1.4 \text{ }^\circ\text{C}$ , respectively.

Simultaneous time measurements of cusps distance variation, temperature and photo-diode signal for MOD cavities restored with SDR flow + are reported in figure 4. The photo-diode signal is reported in an arbitrary scale and it is used to detect the light curing and the dark reaction phases. For both the bulk fill (Fig. 4a) and incremental (Fig. 4b) techniques a delay is observed in the cusps distance variation before a steep contraction occurs.

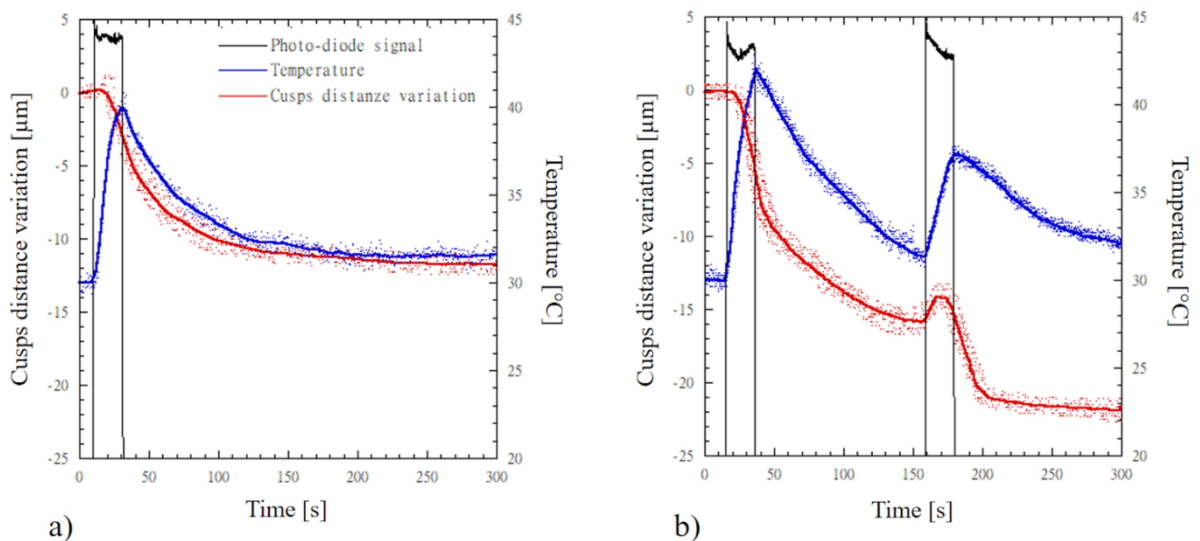


**Figure 4.** Simultaneous time measurements of cusps distance variation, temperature and photo-diode signal for MOD cavities restored with SDR flow plus. The photo-diode signal is reported in an arbitrary scale and it is used to detect the light curing and the dark reaction phases. MOD cavities restored according to: a) the bulk-fill technique; b) the incremental technique.

A steep cusps distance variation is observed for both the bulk fill and incremental techniques during the light curing phase, and cusps distance variation still occurs at a lower steepness through the dark reaction phase (Figure 4). For the incremental technique, a further steep cusps distance variation is observed as the second composite layer undergoes polymerization. Table 4 reports mean values and standard deviation of cusps distance variation of MOD cavities restored with SDR flow + computed after 300 s and 3600 s. Cusps distance variation measured for tooth restored through the incremental technique ( $21.8 \pm 1.9 \mu\text{m}$ ) is higher than that measured for tooth restored through the bulk fill technique ( $11.8 \pm 3 \mu\text{m}$ ), however the difference between the means is not statistically significant ( $p=0.12$ ). Temperature rise observed for SDRB and SDRI are  $9.5 \text{ }^\circ\text{C} \pm 1.7 \text{ }^\circ\text{C}$  and  $11.9^\circ\text{C} \pm 1.7 \text{ }^\circ\text{C}$ , respectively.

#### **4. Discussion**

Bulk fill composites have been particularly used in deep cavities, as they reduce the number of steps required for restoration. Bulk fill composites are not significantly different from conventional composites in terms of microleakage [1, 32]. Two types of bulk fill materials (SDR flow plus and SonicFill 2) have been used in our bulk fill groups. SDR has an amount of organic matrix higher than Sonic Fill (Table 1).

The mean shrinkage values (Figure 2) at 3600 s for SDR and SFL are  $0.925 \pm 0.041$   $\mu\text{m}/\mu\text{m}\%$  and  $0.523 \pm 0.029$   $\mu\text{m}/\mu\text{m}\%$ , respectively. Of course, the higher shrinkage of SDR is directly related to the amount of the polymeric matrix. It is worth to note that at 3600 s both the bulk fill composites show a positive steepness for the shrinkage profile (Figure 2), thus suggesting that shrinkage continues to increase. By using the equation reported by Garcia et al. [19], mean values of volumetric shrinkage of SDR and SFL are 2.75 % and 1.56 %, respectively. These volumetric shrinkage values are consistent but slightly lower than those measured for SDR and SFL with a linometer [19, 20]. Instead, the volumetric shrinkage of 1.56 % computed for SFL is consistent with that measured with a 3D camera imaging system [18]. Differences between our results and those reported in the literature may depend on several factors such as the technique adopted to measure shrinkage, the light curing energy provided for polymerization, and also on the time point at which shrinkage is measured. Shrinkage of light cured restorative materials is a very complex phenomenon as the contraction differs along the three-dimensional directions, thus leading to an anisotropic shrinkage [33, 34]. We measured shrinkage in the direction orthogonal to the light front through strain gauge based extensometer (Figure 1a) as this configuration better represents, in vitro, deformation occurring on the lingual and vestibular cusps of the restored MOD cavity (Figure 1c). Shrinkage measured in the direction orthogonal to the light front is lower than that measured in the axial direction of the light front through the linometer or the bonded disc method [34], as shrinkage of deep composite layers, undergoing a

polymerization kinetics lower than the surface layer [1, 35, 36], provide a significant contribution to the contraction measured in the axial direction.

Compressive properties of RBCs are of great importance as the stress due to mastication, acting on restored teeth, is mainly of compressive nature. The compressive strength and Young's modulus in compression measured for SFL, significantly higher ( $p < 0.05$ ) than those observed for SDR (Table 3), are directly ascribed to the amount of the filler reinforcement phase (Table 1). It is worth to note that similarly to shrinkage also compressive properties largely depend on the time point at which properties are measured. For both the investigated bulk-fill composites, significantly higher strength and stiffness ( $p < 0.05$ ) have been observed after 72 h (Table 3). The compressive strength values measured for SDR and SFL are consistent with values reported in literature [22, 23]. At both time points, SFL shows a compressive strength and Young's modulus significantly higher ( $p < 0.05$ ) than those recorded for SDR. Instead, at both time points, strain to failure of SFL is significantly lower ( $p < 0.05$ ) than that measured for SDR. The difference in mechanical properties observed for the two bulk fill composites suggests that SFL is stiffer and more brittle than SDR, while SDR is more compliant than SFL.

Although a wide literature has been developed regarding in vitro experimental cusps deflection as conventional RBCs are used to restore MOD cavities of premolars [6, 25-30], little is known on cusps deflection as bulk-fill composites are used for restoring MOD cavities of premolars according to the incremental or to the bulk-fill techniques. Kim et al. [31] recently evaluated cusp deflection of aluminium teeth [6]

according to a variety of conventional and bulk-fill composites considering both the incremental and the bulk-fill techniques, and a reduction in cusp deflection from bulk to incremental layering has been observed. Similarly to shrinkage (Figure 2) and compressive properties (Table 3), also cusp distance variation (Table 4) depends on the time point at which measurements are taken. For each type of bulk fill composite and layering technique, cusp distance variation values at 3600 s are higher than those measured at 300 s. According to the bulk-fill technique, mean values of cusps distance variation measured at 3600 s for SFLB and SDRB are 22.9  $\mu\text{m}$  and 20.8  $\mu\text{m}$ , respectively. These values are between the mean values measured for the same bulk-fill composite, considering aluminium rectangular cusps having 1 mm and 2 mm thickness [31]. Cusps deflection depends on bending stiffness, thus it directly depends on the product between the second moment of area and the Young's modulus. The mean width value of our premolar cusps (Table 2) is 6.47 mm, significantly lower than the aluminium cusps (8 mm) adopted by Kim et al. Moreover, the shape of dental cusps cross-section is semi-elliptical, hence the second moment of area is lower than that of rectangular cross-section having similar dimension. Additionally, the Young's modulus of aluminium is about thrice that of dentine. For all these reasons, even if the mean cusps thickness of our premolar cusps is 3.03 mm (Table 2), the bending stiffness of our premolar cusps is much lower than the bending stiffness of the aluminium teeth having similar thickness. Therefore, cusps distance variations measured at 3600 s (Table 4) are consistent with deflection of aluminium cusps measured by Kim et al. On the other hand, the mean value of cusps distance variation measured for SFL (22.9  $\mu\text{m}$ )

is consistent with the mean value (24.3  $\mu\text{m}$ ) recorded for MOD restoration of human premolars by Nguyen et al. [37].

For SFL composite no significant difference in cusps distance variation has been observed between the bulk-fill and the incremental layering techniques ( $p=0.89$ ). Also for the SDR composite no significant difference in cusps deflection has been observed for the bulk-fill or the incremental layering techniques ( $p=0.43$ ).

Although a lower cusps distance variation would be expected for SFL, as shrinkage values of SFL are significantly lower ( $p<0.05$ ) than SDR (Figure 2), no significant difference in cusps deflection between SFLB and SDRB has been observed ( $p=0.99$ ). Similarly, no significant difference in cusps deflection between SFLI and SDRI has been observed ( $p=1,00$ ). The Young's Modulus of the SDR is significantly lower than SFL (Table 3), thus it promotes elastic deformation of the material. SDR is more compliant than SFL, thus it reduces the amount of stress on the cavity wall as the composite shrinks. Instead, the SFL composite generates high stress at cavity walls because of the higher stiffness, but this stress is compensated by the lower shrinkage of this composite. Therefore, dental cusps deflection for MOD cavities depends on both shrinkage and mechanical properties. High viscous composites (e.g. SFL), characterised by low shrinkage and high stiffness, produce similar cusps deflection of low viscous composites (e.g. SDR), characterised by high shrinkage and low stiffness.

Concerning the bulk-fill technique (Figure 3a and 4a), temperature rise mean values span from 8.2  $^{\circ}\text{C}$  to 9.5  $^{\circ}\text{C}$ , and higher temperature levels have been recorded for the flowable composite SDR. However, the difference between the mean values

recorded for the different composites is not significant ( $p=0.92$ ). Similarly, for the incremental layering technique (Figure 3b and 4b), temperature rise values recorded through the first increment span from 9.5 °C to 11.9 °C, and higher temperature levels have been recorded for the flowable composite SDR. However, difference between the mean values recorded for the different composites is not significant ( $p=0.99$ ). Karacan and Ozyurt have recorded similar temperature increase values with thermocouples placed 1 mm below the MOD cavity and using a high viscosity bulk-fill composite [1, 38]. Temperature rise occurring in the core of SDR composite, higher than 20 °C, has been measured using different techniques [7, 17, 39]. These temperature levels would be detrimental for the pulp tissue. Fortunately, dentin acts as a thermal insulator system since thermal conductivity of dentin [40] effectively reduces temperature rise occurring in the pulp. Therefore, for both SDR and SFL composites the light curing modality of 1000 mW/cm<sup>2</sup> for 20 s can be considered thermally safe if an appropriate thickness of occlusal dentin is preserved [38, 41 – 43].

Since no significant difference has been observed for both cusp distance variation and temperature rise, according to the different restorative materials and layering techniques, the null hypothesis has been rejected.

## **5. Conclusions**

Based on the reported results the following conclusions can be drawn:

- Shrinkage of SDR is significantly higher ( $p<0.05$ ) than Sonic Fill, while the strength and the Young's modulus of Sonic Fill are significantly higher ( $p<0.05$ ) than SDR.

- For both SDR and Sonic Fill composites, no significant difference ( $p=0.95$  and  $p=0.12$ , respectively) has been observed for cusps distance variation according to MOD cavities restored through the bulk-fill or the incremental layering techniques.

- Although a lower cusps distance variation would be expected for Sonic Fill, as shrinkage values of Sonic Fill are lower than SDR, no significant difference in cusps deflection between Sonic Fill and SDR has been observed according to both the bulk fill and the incremental layering technique. This result can be ascribed to the Young's modulus suggesting that Sonic Fill is stiffer than SDR, while SDR is more compliant than Sonic Fill.

- Temperature rise levels are below  $11.9\text{ }^{\circ}\text{C}$ , however no significant difference in the mean values of temperature rise has been observed between the bulk-fill composites and the layering techniques.

- The curing modality ( $1000\text{ mW/cm}^2$  for 20 s) can be considered thermally safe for the pulp tissue if the thickness of the occlusal dentin is not lower than 1 mm.

## **References**

1. De Santis R.; Lodato V.; Gallicchio V.; Prisco D.; Riccitiello F.; Rengo S.; Rengo C. Cuspal Deflection and Temperature Rise of MOD Cavities Restored through the Bulk-Fill and Incremental Layering Techniques Using Flowable and Packable Bulk-Fill Composites. *Materials*. 2020; 13(24), 5664.
2. Braga R.R.; Ballester R.Y.; Ferracane J.L. Factors involved in the development of polymerization shrinkage stress in resin-composites: a systematic review. *Dental materials*. 2005; 21(10):962-70.

3. De Santis R.; Gloria A.; Prisco D.; Prisco D.; Amendola E.; Puppulin L.; Pezzotti G.; Rengo S.; Ambrosio L.; Nicolais L. Fast curing of restorative materials through the soft light energy release. *Dental Materials*. 2010; 26(9):891-900.
4. Pashley D.H. Clinical considerations of microleakage. *Journal of endodontics*. 1990; 16(2):70-7.
5. De Santis R.; Mollica F.; Prisco D.; Rengo S.; Ambrosio L.; Nicolais L. A 3D analysis of mechanically stressed dentin–adhesive–composite interfaces using X-ray micro-CT. *Biomaterials*. 2005; 26(3):257-70.
6. Kwon Y.; Ferracane J.; Lee I.B. Effect of layering methods, composite type, and flowable liner on the polymerization shrinkage stress of light cured composites. *Dental materials*. 2012; 28(7):801-9.
7. Kim R.J.; Son S.A.; Hwang J.Y.; Lee I.B.; Seo D.G. Comparison of photopolymerization temperature increases in internal and external positions of composite and tooth cavities in real time: incremental fillings of microhybrid composite vs. bulk filling of bulk fill composite. *Journal of Dentistry*. 2015; 43(9):1093-8.
8. Ilie N.; Bucuta S.; Draenert M. Bulk-fill resin-based composites: an in vitro assessment of their mechanical performance. *Operative dentistry*. 2013; 38(6):618-25.
9. Chesterman J.; Jowett A.; Gallacher A.; Nixon P. Bulk-fill resin-based composite restorative materials: a review. *British Dental Journal*. 2017; 222(5):337.

10. Lima R.B.; Troconis C.C.; Moreno M.B.; Murillo-Gomez F.; De Goes M.F. Depth of cure of bulk fill resin composites: A systematic review. *Journal of Esthetic and Restorative Dentistry*. 2018; 30(6):492-501.
11. Hirata R.; Kabbach W.; De Andrade O.S.; Bonfante E.A.; Giannini M.; Coelho P.G. Bulk fill composites: an anatomic sculpting technique. *Journal of Esthetic and Restorative Dentistry*. 2015; 27(6):335-43.
12. El-Safty S.; Akhtar R.; Silikas N.; Watts D.C. Nanomechanical properties of dental resin-composites. *Dental Materials*. 2012; 28(12):1292-300.
13. Swift Jr E.J. Bulk-fill Composites, Part I. *Journal of Esthetic and Restorative Dentistry*. 2015; 27(3):176-9.
14. Sommer A.P.; Gente M. Light-induced control of polymerization shrinkage of dental composites by generating temporary hardness gradients. *Biomedizinische Technik. Biomedical engineering*. 1999; 44(10):290-3.
15. Chen T.Y.; Huang P.S.; Chuang S.F. Modeling dental composite shrinkage by digital image correlation and finite element methods. *Optics and Lasers in Engineering*. 2014; 61:23-30.
16. De Santis R.; Gloria A.; Sano H.; Amendola E.; Prisco D.; Mangani F.; Rengo S.; Ambrosio L.; Nicolais N. Effect of light curing and dark reaction phases on the thermomechanical properties of a Bis-GMA based dental restorative material. *Journal of Applied Biomaterials and Biomechanics*. 2009; 7(2):132-40.

17. Ibarra E. Physical properties of a new sonically placed composite resin restorative material. Uniformed Services University of the Health Sciences Bethesda United States. 2013.
18. Kim R.J.; Kim Y.J.; Choi N.; Lee I. Polymerization shrinkage, modulus, and shrinkage stress related to tooth-restoration interfacial debonding in bulk-fill composites. *Journal of dentistry*. 2015; 43.4: 430-439.
19. Garcia D.; Yaman P.; Dennison J.; Neiva G.F. Polymerization shrinkage and depth of cure of bulk fill flowable composite resins, *Operative Dentistry*. 2014; 39-4, 441-448.
20. Son S.A.; Park J.; Seo D.; Ko C.C.; Kwon Y.H. How light attenuation and filler content affect the microhardness and polymerization shrinkage and translucency of bulk-fill composites. *Clinical Oral Investigations*. 2017; 21,559–565.
21. Didem A.; Gozde Y.; Nurhan O. Comparative mechanical properties of bulk-fill resins. *Open Journal of Composite Materials*. 2014; 4, 117 - 121.
22. Vandana S.; Bhat G.; Hedge M. Comparative evaluation of flexural and compressive strengths of bulk-fill composites. *International Journal of Advanced Scientific and Technical Research*. 2017.
23. Algamaiah H.; Sampaio C.S.; Rigo L.C.; Janal M.N.; Giannini M.; Bonfante E.A.; Coelho P.G.; Reis A.F.; Hirata R. Microcomputed Tomography Evaluation of Volumetric Shrinkage of Bulk-Fill Composites in Class II Cavities. *Journal of Esthetic and Restorative Dentistry*. 2017; 29(2):118-27.

24. Sakaguchi R.L.; Wiltbank B.D.; Shah N.C. Critical configuration analysis of four methods for measuring polymerization shrinkage strain of composites. *Dental Materials*. 2004; 20(4):388-96.
25. Tiba A.; Charlton D.G.; Vandewalle K.S.; Ragain Jr J.C. Comparison of two video-imaging instruments for measuring volumetric shrinkage of dental resin composites. *Journal of dentistry*. 2005; 33(9):757-63.
26. Behery H.; El-Mowafy O.; El-Badrawy W.; Saleh B.; Nabih S. Cuspal deflection of premolars restored with bulk-fill composite resins. *Journal of Esthetic and Restorative Dentistry*. 2016; 28(2):122-30.
27. Suliman A.A.; Boyer D.B.; Lakes R.S. Cusp movement in premolars resulting from composite polymerization shrinkage. *Dental Materials*. 1993; 9(1):6-10.
28. Fleming G.J.; Khan S.; Afzal O.; Palin W.M.; Burke F.J.T. Investigation of polymerisation shrinkage strain, associated cuspal movement and microleakage of MOD cavities restored incrementally with resin-based composite using an LED light curing unit. *Journal of dentistry*. 2007; 35(2):97-103.
29. Alomari Q.D.; Reinhardt J.W.; Boyera D.B. Effect of liners on cusp deflection and gap formation in composite restorations. *Operative Dentistry*. 2001; 26(4):406-11.
30. Kim Y.J.; Kim R.; Ferracane J.L.; Lee I.B. Influence of the compliance and layering method on the wall deflection of simulated cavities in bulk-fill composite restoration. *Operative dentistry*. 2016; 41(6):e183-e194.

31. Al-Ahdal K.; Silikas N.; Watts D.C. Rheological properties of resin composites according to variations in composition and temperature. *Dental Materials*. 2014; 30(5):517-24.
32. Mosharrafian S.; Heidari A.; Rahbar P. Microleakage of two bulk fill and one conventional composite in class II restorations of primary posterior teeth. *Journal of dentistry (Tehran, Iran)*. 2017; 14(3):123.
33. Lee I.B.; Cho B.H.; Son H.H.; Um C.M.; Lim B.S. The effect of consistency, specimen geometry and adhesion on the axial polymerization shrinkage measurement of light cured composites. *Dental Materials*. 2006; 22(11):1071-9.
34. Ferracane J.L.; Hilton T.J.; Stansbury J.W.; Watts D.C.; Silikas N.; Ilie N.; Heintze S.; Cadenaro M.; Hickel R. Academy of Dental Materials guidance-Resin composites: Part II-Technique sensitivity (handling, polymerization, dimensional changes). *Dental Materials*. 2017; 33(11):1171-91.
35. Krifka S.; Hiller K.A.; Bolay C.; Petzel C.; Spagnuolo G.; Reichl F.X.; Schmalz G.; Schweikl H. Function of MAPK and downstream transcription factors in monomer-induced apoptosis. *Biomaterials*. 2012; 33(3):740-50.
36. Eckhardt A.; Müller P.; Hiller K.A.; Krifka S.; Bolay C.; Spagnuolo G.; Schmalz G.; Schweikl H. Influence of TEGDMA on the mammalian cell cycle in comparison with chemotherapeutic agents. *Dental Materials*. 2010; 26(3):232-41.
37. Nguyen K.V.; Wong R.H.; Palamara J.; Burrow M.F. The effect of resin-modified glass-ionomer cement base and bulk-fill resin composite on cuspal deformation. *Operative dentistry*. 2016; 41(2):208-18.

38. Karacan A.O.; Ozyurt P. Effect of preheated bulk-fill composite temperature on intrapulpal temperature increase in vitro. *Journal of Esthetic and Restorative Dentistry*. 2019; 31:583–588.
39. Vinagre A.; Ramos J.; Alves S.; Messias A.; Alberto N.; Nogueira R. Cuspal displacement induced by bulk fill resin composite polymerization: biomechanical evaluation using fiber Bragg grating sensors. *International Journal of Biomaterials*. 2016; (3):1-9.
40. De Magalhaes M.F.; Ferreira R.A.; Grossi P.A.; de Andrade R.M. Measurement of thermophysical properties of human dentin: effect of open porosity. *Journal of Dentistry*. 2008; 36(8):588-94.
41. Yasa E.; Atalayin C.; Karacolak G.; Sari T.; Turkun S. Intrapulpal temperature changes during curing of different bulk-fill restorative materials. *Dental Materials Journal*. 2017; 36(5):566-572.
42. Nocca G.; Callà C.; Martorana G.E.; Cicillini L.; Rengo S.; Lupi A.; Cordaro M.; Gozzo M.L.; Spagnuolo G. Effects of dental methacrylates on oxygen consumption and redox status of human pulp cells. *BioMed Research International*. 2014; 2014:956579.
43. Krifka S.; Petzel C.; Bolay C.; Hiller KA.; Spagnuolo G.; Schmalz G.; Schweikl H. Activation of stress-regulated transcription factors by triethylene glycol dimethacrylate monomer. *Biomaterials*. 2011; 32(7):1787-95.



<b>Dottorando</b>	<b>Dr. Vito Gallicchio</b>
<b>Università</b>	<b>Università degli Studi di Napoli Federico II</b>
<b>Corso di Dottorato</b>	<b>Dottorato di Ricerca in Medicina Clinica e Sperimentale</b>
<b>Ciclo</b>	<b>34°</b>
<b>Referente universitario per il Progetto / Tutor</b>	<b>Prof. Vincenzo D'Antò</b>
<b>Coordinatore del Corso</b>	<b>Prof. Francesco Beguinot</b>
<b>Data Avvio Attività</b>	<b>26/11/2018</b>
<b>CUP</b>	<b>E66C18000900002</b>
<b>Titolo Progetto</b>	<b>Progettazione di strutture 3D avanzate custom-made con specifiche proprietà magnetiche per la rigenerazione guidata del tessuto osseo</b>

La borsa di dottorato è stata cofinanziata con risorse del POR Campania FSE 2014-2020 ASSE III - "Dottorati di Ricerca con Caratterizzazione Industriale" – D.D. n.155 del 17.05.2018 - CUP E66C18000900002 - CML OP\_7741 18062AP000000001

